

Enrichment of Heavy Elements in the red giant S 15–19 in the Sextans Dwarf Spheroidal Galaxy*

Satoshi HONDA

Kwasan Observatory, Kyoto University, Ohmine-cho Kita Kazan, Yamashina-ku, Kyoto 607-8471

honda@kwasan.kyoto-u.ac.jp

Wako AOKI, Nobuo ARIMOTO

National Astronomical Observatory of Japan, 2-21-1 Osawa, Mitaka, Tokyo 181-8588

Department of Astronomical Science, The Graduate University of Advanced Studies, Mitaka, Tokyo

181-8588

aoki.wako@nao.ac.jp, arimoto.n@nao.ac.jp

and

Kozo SADAKANE

Astronomical Institute, Osaka Kyoiku University, 4-698-1 Asahigaoka, Kashiwara-shi, Osaka

582-8582

sadakane@cc.osaka-kyoiku.ac.jp

(Received 2010 December 2; accepted 2010 December 20)

Abstract

We determined chemical abundances of the Extremely Metal-Poor (EMP) star S 15–19 ($[\text{Fe}/\text{H}] = -3.0$) in the Sextans dwarf galaxy. While heavy neutron-capture elements (e.g., Ba) are generally deficient in EMP stars in dwarf galaxies, this object was shown to have an exceptional over-abundance of Ba ($[\text{Ba}/\text{Fe}] \sim +0.5$) by a previous study, which is similar to those of r-process-enhanced stars found in the field halo. Our new high-resolution spectroscopy for this object for the blue region, however, reveals that no clear excess of r-process elements, like Eu, appears in this object. Moreover, a significant excess of carbon ($[\text{C}/\text{Fe}] = +1.0$) and a deficiency of Sr ($[\text{Sr}/\text{Fe}] = -1.4$) are found for this object. Taking the variation of radial velocities measured at the two different epochs into consideration, the origin of the excesses of heavy neutron-capture elements in S 15–19 is not the r-process, but is the s-process in an asymptotic giant branch (AGB) star that was the binary companion (primary) of this object. Carbon- and s-process-enhanced material should have been transferred to the surface of S 15–19 across the binary system. These results are compared with carbon-enhanced metal-poor stars in the field halo.

Key words: nuclear reactions, nucleosynthesis, abundance – stars: abundances – galaxies: dwarf – stars: individual (Sextans S 15–19)

1. Introduction

Dwarf galaxies around the Milky Way (MW) are believed to provide a key to understanding the formation processes of the MW halo structure and chemical evolution in small galaxies (e.g., Mateo et al. 1998; Tolstoy et al. 2009). In order to determine the chemical composition of individual stars of dwarf galaxies, high-resolution spectroscopy has been obtained for red giants in some nearby dwarf spheroidals with 8-10m class telescopes in the past decade.

While a large sample of red giants have been studied for some dwarf spheroidal galaxies (e.g., Fornax: Letarte et al. 2010), abundance measurements of extremely metal-poor (EMP) stars ($[\text{Fe}/\text{H}] \lesssim -3$) are still quite limited. A few EMP stars have been studied by Shetrone, Côté, & Sergent (2001), Fulbright, Rich, & Castro (2004), and Sadakane et al. (2004). Recently, the chemical compositions of EMP stars in the Sextans dwarf galaxy found by Helmi et al. (2006) were studied in detail by Aoki et al. (2009). The sample of EMP stars in dwarf galaxies studied by high-resolution spectroscopy has been increasing owing to recent work Cohen & Huang (2009) and Cohen & Huang (2010) for Draco and Ursa Minor. An EMP star with $[\text{Fe}/\text{H}] = -3.7$ was discovered in the Sculptor dwarf galaxy by Frebel, Kirby, & Simon (2010). Moreover, EMP stars have been discovered in the so-called Ultra Faint dwarf Galaxies (UFdG), for which abundance measurements with high-resolution spectroscopy have been made only quite recently (see below).

These studies suggest that the abundance ratios of α -elements to Fe (e.g., Mg/Fe) of EMP stars in most dwarf galaxies are as high as those of halo field stars, while the ratios are sometimes significantly lower at higher metallicity. However, low α/Fe ratios are at least found in EMP stars of Sextans (Aoki et al. 2009), and further studies for a larger sample are required to derive any conclusion on the origins of the chemical composition of these EMP stars.

Another interesting feature found by previous studies for very metal-poor stars ($[\text{Fe}/\text{H}] \lesssim -2.5$) in dwarf galaxies is the low abundances of heavy neutron-capture elements. While some stars with overabundances of Ba ($[\text{Ba}/\text{Fe}] > 0$) were found by Shetrone, Côté, & Sergent (2001) for $[\text{Fe}/\text{H}] \gtrsim -2$, no such object with lower metallicity exists in their sample. Fulbright, Rich, & Castro (2004) and Sadakane et al. (2004) reported extremely metal-poor ($[\text{Fe}/\text{H}] \sim -3$) stars with strikingly low Ba abundances ($[\text{Ba}/\text{Fe}] < -2.6$ for Draco 119, and $[\text{Ba}/\text{Fe}] = -1.3$ for Ursa Minor COS 4, respectively). Low Ba (and Sr) abundances have also been found by more recent studies of dwarf galaxy stars (Aoki et al. 2009; Cohen & Huang 2010) as well as for UFdGs (Frebel et al. 2010; Simon et al. 2010).

This makes a clear contrast to the neutron-capture elements in MW EMP stars, in which a very large dispersion of the abundances of heavy elements with respect to Fe is seen (e.g., McWilliam et al. 1995; Honda et al. 2004; François et al. 2007). The abundance

* Based on data collected at Subaru Telescope, which is operated by the National Astronomical Observatory of Japan.

patterns of heavy elements in EMP stars in the field halo that show over-abundances of neutron-capture elements are usually similar to the solar-system r-process pattern (e.g., Sneden et al. 2003). This is interpreted as being a result of the short time-scale of the enrichment by the r-process events compared to s-process enrichment by evolved intermediate-mass stars (AGB stars), although the astrophysical site of the r-process is still not well understood. On the other hand, a large fraction of carbon-enhanced metal-poor (CEMP) stars also show an enhancement of neutron-capture elements (Aoki et al. 2007). The origin of heavy elements of these objects is the s-process in metal-poor AGB stars, even at low metallicity. Such objects are interpreted as being a result of mass transfer from a companion that was previously an AGB star, and has been provided with carbon-rich material with a large excesses of heavy neutron-capture elements produced by the s-process during AGB evolution (Busso et al. 1999).

Among the EMP stars in dwarf galaxies studied so far, the red giant S 15–19 in Sextans has an exceptionally high Ba abundance ($[\text{Ba}/\text{Fe}] = +0.5$; Aoki et al. 2009). The value is as high as those of the r-process-enhanced stars in the field halo (r-II stars: Beers & Christlieb 2005). If the origin of the Ba excess in S 15–19 is the r-process, this indicates that a large scatter of neutron-capture elements also appears in dwarf galaxies, as found in the field halo. However, no constraint on the origin of heavy elements of this object was obtained by a previous study (Aoki et al. 2009) because no other neutron-capture element was measured due to the limited wavelength coverage and data quality.

In order to determine the origins of heavy elements in S 15–19 in Sextans, we obtained a new blue spectrum with higher quality, and conducted detailed chemical abundance measurements. This paper reports on the result of our abundance study, and discusses the enrichment processes of this object.

2. Observations and Measurements

High resolution spectroscopy was carried out for S 15–19 on 2010 Feb. 9 using Subaru/HDS (Noguchi et al. 2002). The spectrum covers 3760–5490 Å with a resolving power of 40,000 by 2×2 on-chip binning. This spectral range includes atomic lines of Eu, Sr, and CH molecular bands, which were not covered by a previous study (4400–7100 Å: Aoki et al. 2009). The echelle data were processed using the IRAF software echelle package¹ in a standard manner. The long exposure (8 hr) collected 980 photons per 1.8 km s^{-1} pixel at 4500 Å. The spectrum is, however, significantly affected by the sky background. The sky spectrum was extracted from the region around the object on the slit, and subtracted. The signal-to-noise (S/N) ratio of the spectrum after sky subtraction was 25 (per resolution element) at 4500 Å.

Equivalent widths were measured by fitting Gaussian profiles. The derived equivalent

¹ IRAF is distributed by the National Optical Astronomy Observatories, which is operated by the Association of Universities for Research in Astronomy, Inc. under cooperative agreement with the National Science Foundation.

widths are given in table 1. Most of the line data were taken from the list of Aoki et al. (2009) and Aoki et al. (2005). The equivalent widths are compared with the previous measurements of Fe I lines (Aoki et al. 2009) for the overlapping wavelength range (4400 – 5490 Å) in figure 1. The results of the present work are slightly larger (by 6%) than those of Aoki et al. (2009). However, the discrepancy is smaller than the measurement errors (13 mÅ for a S/N \sim 25 spectrum), indicating no evident systematic difference in the equivalent widths between the two studies.

A measurement of radial velocity was made for selected clean iron lines used in the equivalent-width measurements. The derived radial velocity is 223.60 ± 0.23 km s $^{-1}$. This value is by 3 km s $^{-1}$ different from that obtained by a previous study (226.05 ± 0.11 km s $^{-1}$: Aoki et al. 2009), suggesting that S 15–19 belongs to a binary system.

3. Abundance Analysis and Results

Chemical abundance analyses were performed using the analysis program SPTOOL developed by Y.Takeda (Takeda 2005 private communication), based on Kurucz’s ATLAS9/WIDTH9 (Kurucz 1993). We computed spectra and equivalent widths based on model atmospheres under the assumption of local thermodynamic equilibrium (LTE).

We adopted the model atmosphere parameters (effective temperature, gravity, micro-turbulent velocity, and metallicity) derived by a previous study (Aoki et al. 2009), which are $T_{\text{eff}}=4600\text{K}$, $\log g=1.2$, $v_{\text{micro}}=2.6\text{km s}^{-1}$, and $[\text{Fe}/\text{H}]=-3.1$. We used the equivalent widths obtained by this work and Aoki et al. (2009) for the abundance analysis.

The abundances of Fe I and Fe II (Ti I and Ti II) derived with these atmospheric parameters are in good agreement, confirming the adopted $\log g$ value. The iron abundance of this star ($[\text{Fe}/\text{H}] = -3.05$) was derived from Fe I and Fe II lines. We here adopt the Asplund et al. (2009) solar abundances.

3.1. Neutron-capture elements

The two resonance lines of Ba II at 4554 Å and 4934 Å were measured by the present analysis, in addition to the two lines in the red region (5853 Å and 6141 Å) measured by Aoki et al. (2009). The effects of a hyperfine splitting and isotope shifts are significant in the abundance analysis of Ba, particularly for the strong resonance lines. We calculated the Ba abundances, assuming Ba isotope ratios formed by the r-process and s-process, which were estimated from solar-system material (McWilliam 1998; Sneden et al. 2008). We confirmed that the abundances derived from the 4554 Å and 4934 Å assuming r-process isotope ratios are significantly different (0.3 or 0.4 dex) from those derived assuming the s-process one, while the results derived from 5853 Å and 6141 Å are insensitive to the assumed isotope ratios. Therefore, we decided to adopt the Ba abundance determined using the 5853 and 6141 lines, and to use the resonance lines for comparisons. The final result was determined by assuming

the Ba isotope ratios for the s-process case, based on the abundance pattern derived for this object in the following analysis. The derived Ba abundance, given in table 2 ($[\text{Ba}/\text{Fe}]$), agrees well with that of Aoki et al. (2009).

Among lighter neutron-capture elements, we determine the Sr abundance ($[\text{Sr}/\text{Fe}] = -1.4$) from the Sr II 4077 Å line. The under-abundance of Sr is significant given the over-abundance of Ba. Even if a large error in the equivalent width measurement (20 mÅ) for the Sr line is taken into account, the Sr abundance is at most $[\text{Sr}/\text{Fe}] = -1.1$. Hence, the result that Sr is underabundant in this object is robust.

Only upper limits of the abundances were derived for other neutron-capture elements (Y, Zr, La, Ce, Nd, Eu and Dy) using the error estimate for equivalent-width measurements for weak lines provided by Norris et al. (2001) for a given resolution, S/N ratio and sampling. The results were checked by the spectrum-synthesis technique.

Among the neutron-capture elements, the upper limit of the Eu abundance is particularly important to constrain the origin of heavy elements in this object. The upper limit of the Eu abundance $[\text{Eu}/\text{Fe}] < 0.7$ was obtained from the above estimate. However, the spectrum synthesis for the Eu II line at 4129 Å suggests that this is possibly an underestimate (figure 2). We adopt the upper limit $[\text{Eu}/\text{Fe}] < 0.9$ as the final result (table 2).

This results in the upper limit of $[\text{Eu}/\text{Ba}]$ to be $= +0.5$, which is lower than the value expected for the r-process abundance ratio ($[\text{Eu}/\text{Ba}]_{\text{r-process}} = +0.8$: e.g. Burris et al. 2000). The result is rather consistent with the s-process abundance ratio ($[\text{Eu}/\text{Ba}]_{\text{s-process}} = -1.0$), although the constraint is not strong (figure 3).

Hence, the conclusion derived from the upper limit of Eu/Ba is that the Ba excess of S 15–19 is not fully explained by the r-process, but is at least partially contributed by the s-process. The low Sr/Ba ratio ($[\text{Sr}/\text{Ba}] = -1.9$) also supports the significant contribution of the s-process, because a low Sr/Ba ratio is expected from the s-process (in an AGB star) at low metallicity, as a result of very high ratios of neutrons to seed nuclei (Gallino et al. 1998), while the $[\text{Sr}/\text{Ba}]$ value found for r-process-enhanced EMP stars is -0.4 (e.g., CS 22892–052 : Sneden et al. 2003). This suggests that the s-process is the dominant contributor to the heavy neutron-capture elements in S 15–19.

3.2. Other elements

Another support for the s-process contribution is found in the carbon abundance of this object. The carbon abundance was determined by a spectrum synthesis of the CH band at 4324 Å (figure 4), adopting the CH line data from Aoki et al. (2002). The result clearly shows that this star is carbon-enhanced ($[\text{C}/\text{Fe}] = +1.0$), which is a signature of a contribution by AGB nucleosynthesis.

The carbon-isotope ratio was estimated from the CH lines at around 4200 Å, as done by Honda et al. (2004). The derived $^{12}\text{C}/^{13}\text{C}$ ratio is 4 ± 1 , which is a typical value found

in highly evolved red giants (e.g., Charbonel 1995, Spite et al. 2006). Such a low value is also found in some carbon-enhanced metal-poor stars that have low temperature and low gravity (e.g., Ryan et al. 2005).

We also estimate the nitrogen abundance from the CN band at 4215 Å. Although the result is quite uncertain due to the low S/N ratio at this wavelength, a large over-abundance of nitrogen is suggested ($[N/Fe] = +1.5 \pm 0.5$).

3.3. Uncertainties

We estimate the random errors in the analysis, which included the uncertainties of adopted gf values and the equivalent-width measurements, as well as errors due to the uncertainties of stellar parameters adopted in the analysis.

Random errors were estimated from the mean of the standard deviations (1σ) of the abundances derived from individual lines for elements that had three or more lines available (Mg I, Ca I, Ti II, Fe I, and Fe II). We apply this value (0.19 dex) to the species for which only one or two lines have been detected. We adopt 0.3 and 0.5 dex errors for carbon and nitrogen abundances from the CH and CN bands from the estimate by spectrum synthesis.

To estimate the errors due to the uncertainties of stellar parameters, we examine the abundance analysis by changing the parameters, as given in table 3. The change of C abundance due to the T_{eff} change was included in the estimate of the effect on the N abundance determination from the CN band. These errors are not generally very significant, compared with the random errors estimated above.

4. Discussion

Our chemical-abundance measurements for the red giant S 15–19 in the Sextans dwarf spheroidal revealed that this star has excesses of carbon ($[C/Fe] = +1$) and Ba ($[Ba/Fe] = +0.4$) but shows no clear excess of r-process elements ($[Eu/Ba] < +0.5$). A radial velocity variation was found between the two epochs of the past observing. This indicates that the excess of Ba in this star can be attributed to the s-process in an AGB star that was a companion (primary) of the binary to which S 15–19 belongs; also, carbon-rich material has been transferred from the AGB star across the binary system. The low Sr/Ba ratio ($[Sr/Ba] = -1.9$) also suggests the s-process at very low metallicity, which efficiently yields heavier neutron-capture elements due to high neutron-to-seed nuclei ratios (Gallino et al. 1998). Hence, we conclude that this object is a CEMP star with excesses of s-process elements (CEMP-s: Beers & Christlieb 2005).

Figure 5 compares the carbon and Ba abundances of this object with those of Milky Way field stars, where carbon-enhanced stars are emphasized (Aoki 2010). A large number of CEMP stars in the field halo show very high carbon and Ba abundances ($[C/Fe] > +2$, $[Ba/Fe] > +2$). The excesses of carbon and Ba of S 15–19 are not as significant as those of these stars. We note that such moderate excesses of carbon and Ba are also found in CS 22892–052, which is the

first example of r-process-enhanced (r-II) stars in the field halo (Snedden et al. 1996). However, the origin of neutron-capture elements of S 15–19 is completely different from this object.

The relatively small excesses of carbon and Ba in S 15–19 suggest that the mass transfer from the AGB star is not as significant as the one that affected the CEMP stars with very high carbon abundances, or the carbon excess has been diluted during the evolution of S 15–19 along the red giant branch (see below).

Among CEMP-s stars in the field halo, CS 30322–023 has similar excesses of carbon and Ba to S 15–19. This object is a carbon-enhanced ($[C/Fe]=+0.6$) extremely metal-poor ($[Fe/H]=-3.4$) star with a moderate Ba excess ($[Ba/Fe]=+0.6$) studied by Masseron et al. (2006) and Aoki et al. (2007). Interesting features of this object are a large enhancement of nitrogen ($[N/Fe]=+2.5$: Aoki et al. 2007; $+2.8$: Masseron et al. 2006) and the low $^{12}C/^{13}C$ ($=4$: Masseron et al. 2006). This suggests that the carbon-enhanced material has been affected by the CNO cycle. While Masseron et al. (2006) suggested that this object could be a thermally pulsing AGB star, because of its low temperature and low gravity, the carbon-enhancement might have originated from the mass transfer from an AGB star, as in the case of other CEMP-s stars, given the variations of radial velocities found during four years (Masseron et al. 2006). The low $^{12}C/^{13}C$ ratio (~ 4) and the high N abundance ($[N/Fe]\sim +1.5$) of S 15–19 suggest that this object has a similar origin to CS 30322–023, although these results are rather uncertain. Whatever the evolutionary stage of S 15–19 and CS 30322–023 is, the similarity suggests that natures of CEMP stars could be common between the field halo and dwarf galaxies.

To derive a definitive conclusion for such discussions, the statistics of carbon-enhanced stars in dwarf galaxies are required. Unfortunately, however, studies of CEMP stars in dwarf galaxies are still quite limited. For Sextans, Aoki et al. (2009) reported a discovery of the CEMP star S 11–36 ($[Fe/H]=-2.9$, $[C/Fe]=+1.9$) with moderate excess of Ba ($[Ba/Fe]=+0.8$). Although their data quality is insufficient to discuss the details of the chemical composition of this object, the existence of such a CEMP star supports the similarity of the stellar population with carbon-excesses between the dwarf galaxy and the field halo.

At higher metallicity, another carbon-enhanced star with large excesses of neutron-capture elements was found in Ursa Minor dwarf spheroidal (the star K: $[Fe/H]=-2.17$, $[Ba/Fe]=+1.37$, $[Eu/Ba]=-0.33$ with strong C_2 bands) by Shetrone, Côté, & Sergent (2001). At lower metallicity, a carbon-enhanced star with no excess of heavy elements was recently discovered in the UFG SEGUE-1 (SEGUE1-7: $[Fe/H]=-3.52$, $[C/Fe]=+2.3$, $[Ba/Fe]<-1.0$) by Norris et al. (2010). Such stars (so-called CEMP-no stars) are also found at extremely low metallicity in the field halo. Even though the origins of CEMP-no stars and CEMP-s stars could be quite different, both populations also seem to appear in dwarf galaxies. Further study to investigate the statistics of CEMP stars in dwarf galaxies, and comparisons with that in the MW halo, will be useful to constrain the formation processes of EMP stars.

S 15–19 is a unique object that shows a definitely large overabundance of Ba among

EMP stars in dwarf galaxies studied to date². Since the origin of Ba of this object turned out to be the s-process, no r-process enhanced EMP star is known at present in dwarf galaxies. This possibly indicates that dwarf galaxy may have a history of the chemical evolution different from MW. However, since the sample size of EMP stars in dwarf galaxies studied with high-resolution spectroscopy is still small, we cannot derive any definitive conclusion. Indeed, the statistics for halo field stars reveals that the fraction of r-process enhanced stars (r-II stars; $[\text{Eu}/\text{Fe}] > +1$) is on the order of 5% (Barklem et al. 2005), while Ba abundances have been measured for about 20 stars with $[\text{Fe}/\text{H}] < -2.5$ in dwarf galaxies, including UFDG (Frebel & Bromm 2010). Further searches for EMP stars and detailed abundance measurements for dwarf galaxies are strongly desired in order to clarify the chemical evolutions of dwarf galaxies and nucleosynthesis of the r-process.

We would like to thank Dr. A. Tajitsu for his help to our observation. This work was supported by a Grant-in-Aid for Science Research from MEXT and JSPS (grant 21740148, 18104003, and 19540240).

References

- Aoki, W. 2010, in IAU Symp., Chemical Abundances in the Universe: Connecting First Stars to Planets, ed. K. Cunha et al. (Dordrecht: Springer) 265, 111
- Aoki, W. et al. 2009, *A&A*, 502, 569
- Aoki, W., Honda, S., Sadakane, K., and Arimoto, N. 2007, *PASJ*, 59, 15L
- Aoki, W. et al. 2005, *ApJ*, 632, 611
- Aoki, W., Norris, J. E., Ryan, S. G., Beers, T. C., & Ando, H. 2002, *PASJ*, 54, 933
- Asplund, M., Grevesse, N., Sauval, A. J., & Scott P. 2009, *ARA&A*, 47, 481
- Barklem, P. S., et al. 2005, *A&A*, 439, 129
- Beers, T. C., & Christlieb, N. 2005, *ARA&A*, 43, 531
- Burris, D. L., Pilachowski, C. A., Armandroff, T. E., Sneden, C., Cowan, J. J., & Roe, H. 2000, *ApJ*, 544, 302
- Busso, M., Gallino, R., & Wasserburg, G. J. 1999, *ARA&A*, 37, 239
- Charbonnel, C. 1995, *ApJL*, 453, L41
- Cohen, J. G., & Huang, W. 2010, *ApJ*, 719, 931
- Cohen, J. G., & Huang, W. 2009, *ApJ*, 701, 1053
- François, P., et al. 2007, *A&A*, 476, 935
- Frebel, A., Simon, J. D., Geha, M., and Wilman, B. 2010, *ApJ*, 708, 560
- Frebel, A., Kirby, E. N., & Simon, J. D. 2010, *Nature*, 464, 72
- Frebel, A., & Bromm, V. 2010, *MNRAS*, submitted (arXiv:1010.1261)

² The exception is S 11–36 that shows a large excess of Ba, though the abundance results are quite uncertain as mentioned in this section (Aoki et al. 2009). This object also has large excess of carbon, suggesting the origin of Ba is also the s-process.

- Fulbright, J. P., Rich, R. M., & Castro, S. 2004, *ApJ*, 612, 447
- Gallino, R., Arlandini, C., Busso, M., Lugaro, M., Travaglio, C., Straniero, O., Chieffi, A., & Limongi, M. 1998, *ApJ*, 497, 388
- Helmi, A. et al. 2006, *A&A*, 651, 121L
- Honda, S., Aoki, W., Kajino, T., Ando, H., Beers, T. C., Izumiura, H., Sadakane, K., & Takada-Hidai, M. 2004, *ApJ*, 607, 474
- Kurucz, R. L. 1993, CD-ROM 13, *ATLAS9 Stellar Atmospheres Programs and 2 km/s Grid* (Cambridge: Smithsonian Astrophys. Obs.)
- Letarte, B., et al. 2010, *A&A*, 523, 17L
- Masseron, T., et al. 2006, *A&A*, 455, 1059
- Mateo, M. L. 1998, *ARA&A*, 36, 435
- McWilliam, A. 1998, *AJ*, 115, 1640
- McWilliam, A., Preston, G. W., Sneden, C., & Searle, L. 1995, *AJ*, 109, 2757
- Noguchi, K. et al. 2002, *PASJ*, 54, 855
- Norris, J. E., Gilmore, G., Wyse, R. F. G., Yong, D., & Frebel, A. 2010, *ApJ*, 722, L104
- Norris, J. E., Ryan, S. G., & Beers, T. C. 2001, *ApJ*, 561, 1034
- Ryan, S. G., Aoki, W., Norris, J. E., & Beers, T. C. 2005, *ApJ*, 635, 349
- Sadakane, K., Arimoto, N., Ikuta, C., Aoki, W., Jablonka, P., & Tajitsu, A. 2004, *PASJ*, 56, 1041
- Shetrone, M. D., Côté, P., & Sargent, W. L. W. 2001, *ApJ*, 548, 592
- Simon, J. D., Frebel, A., McWilliam, A., Kirby, E. N., & Thompson, I. B. 2010, *ApJ*, 716, 446
- Sneden, C., McWilliam, A., Preston, G. W., Cowan, J. J., Burris, D. L., & Armosky, B. J. 1996, *ApJ*, 467, 819
- Sneden, C., et al. 2003, *ApJ*, 591, 936
- Sneden, C., Cowan, J. J., & Gallino, R. 2008, *ARA&A*, 46, 241
- Spite, M., et al. 2006, *A&A*, 455, 291
- Tolstoy, E., Hill, V., & Tosi, M. 2009, *ARA&A*, 47, 371

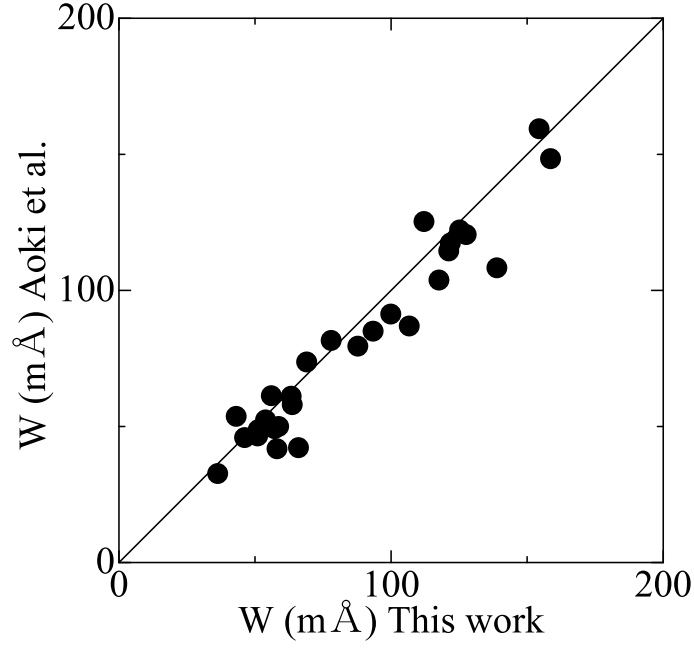


Fig. 1. Comparison of equivalent width (mÅ) measurements by Aoki et al. (2009) and this work.

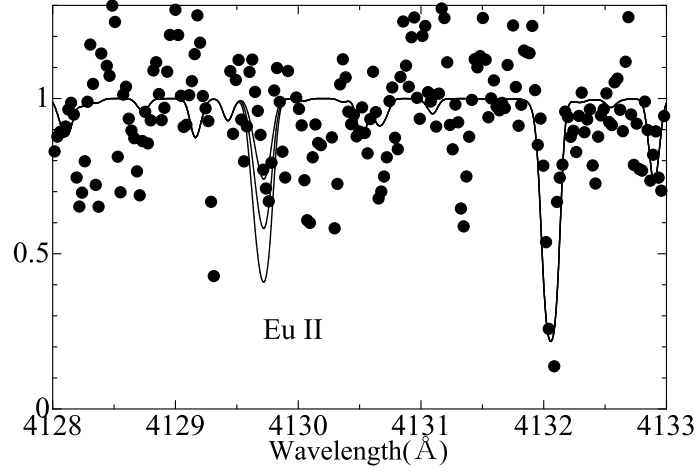


Fig. 2. Spectral region around the Eu feature at 4129 Å for S 15–19. The observed spectrum is shown by filled circles, and synthetic spectra with three Eu abundances ($[\text{Eu}/\text{Fe}] = +0.6, +0.9, +1.2$) are shown by lines. The upper limit of Eu abundance ($[\text{Eu}/\text{Fe}] < +0.9$) is estimated from this comparison.

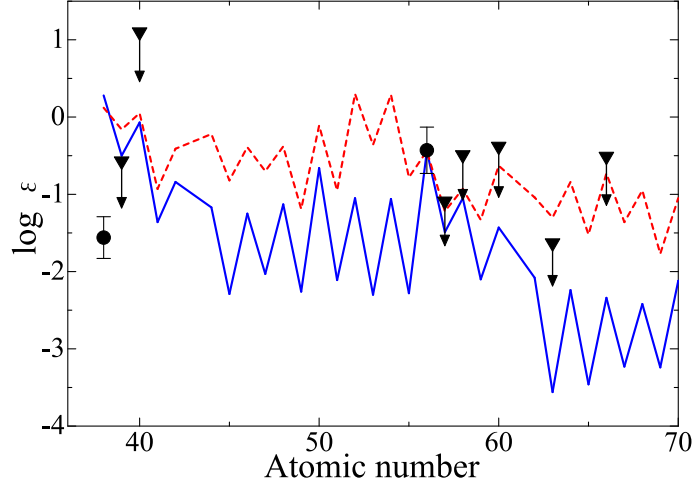


Fig. 3. Abundances of neutron-capture elements (filled circles), or upper limits (triangles), for S 15-19 as a function of the atomic number. The dashed and solid lines are the solar r- and s-process abundance patterns normalized at Ba.

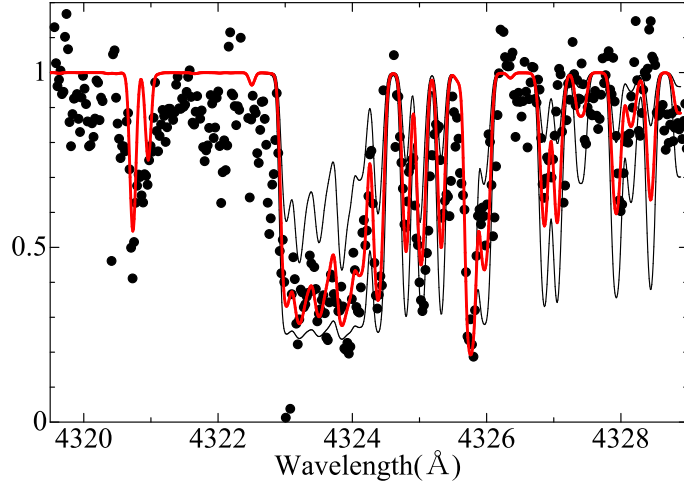


Fig. 4. Spectral region around the CH feature at 4323 Å for S 15-19. The observed spectrum is shown by filled circles, and synthetic spectra with three carbon abundances ($[C/Fe] = +0.5, +1.0, +1.5$) are shown by lines.

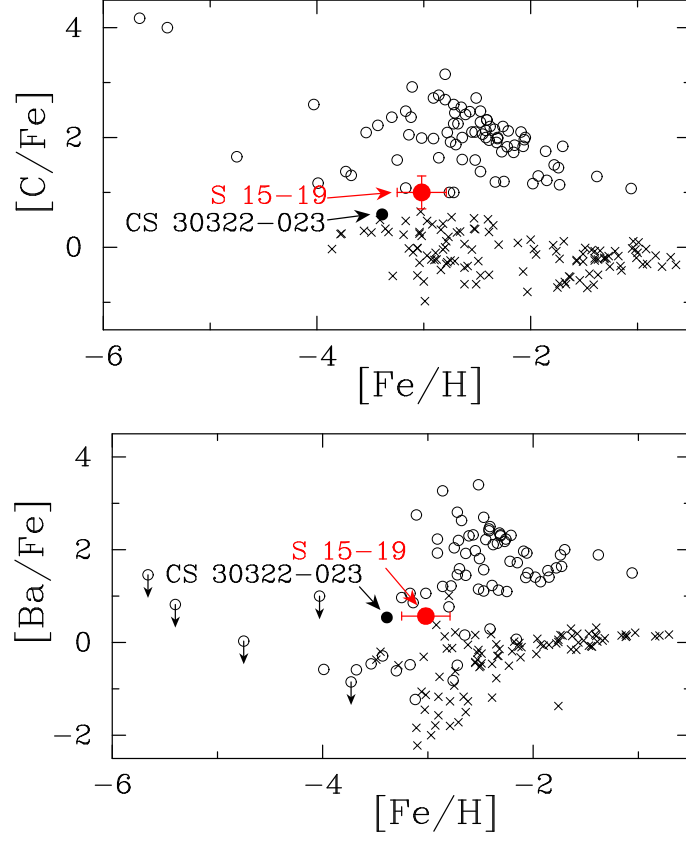


Fig. 5. $[\text{C}/\text{Fe}]$ and $[\text{Ba}/\text{Fe}]$ as a function of $[\text{Fe}/\text{H}]$. Carbon-enhanced stars ($[\text{C}/\text{Fe}] \gtrsim +1$) are shown by open circles, while non-carbon-enhanced stars are shown by crosses (Aoki 2010). S 15-19 is shown by a large filled circle with error bars. CS 30322-023 (a filled circle) is classified into carbon-enhanced object, taking its evolutionary stage and the large nitrogen-enhancement into account (see text).

Table 1. Equivalent Width Measurements

| Species | wavelength(\AA) | L.E.P.(eV) | $\log gf$ | W(m \AA) | $\log \epsilon$ |
|---------|----------------------------|------------|-----------|--------------------|-----------------|
| Na I | 5889.95 | 0.00 | 0.12 | 153.6* | 3.22 |
| Na I | 5895.92 | 0.00 | -0.18 | 137.6* | 3.28 |
| Mg I | 4571.10 | 0.00 | -5.39 | 84.5 | 5.11 |
| Mg I | 4702.99 | 4.33 | -0.38 | 60.3 | 5.04 |
| Mg I | 5172.68 | 2.71 | -0.45 | 203.9 | 5.10 |
| Mg I | 5183.60 | 2.72 | -0.24 | 224.3 | 5.08 |
| Mg I | 5528.40 | 4.35 | -0.34 | 55.4* | 4.90 |
| Ca I | 4318.65 | 1.90 | -0.21 | 48.4 | 3.71 |
| Ca I | 5588.75 | 2.53 | 0.20 | 45.0* | 3.91 |
| Ca I | 6102.72 | 1.88 | -0.79 | 27.1* | 3.78 |
| Ca I | 6122.22 | 1.89 | -0.31 | 40.7* | 3.55 |
| Ca I | 6162.17 | 1.90 | -0.09 | 73.8* | 3.80 |
| Ca I | 6462.57 | 2.52 | 0.31 | 32.5* | 3.53 |
| Sc II | 4246.82 | 0.31 | 0.24 | 156.1 | 0.59 |
| Sc II | 4415.56 | 0.60 | -0.67 | 90.9 | 0.58 |
| Ti I | 4533.24 | 0.85 | 0.53 | 26.2 | 1.81 |
| Ti I | 4981.73 | 0.85 | 0.56 | 47.8* | 2.11 |
| Ti II | 4443.79 | 1.08 | -0.70 | 93.3 | 1.63 |
| Ti II | 4450.48 | 1.08 | -1.45 | 62.9 | 1.99 |
| Ti II | 4468.51 | 1.13 | -0.60 | 110.4 | 1.89 |
| Ti II | 4501.27 | 1.12 | -0.75 | 104.2 | 1.92 |
| Ti II | 4533.97 | 1.24 | -0.77 | 105.5 | 2.09 |
| Ti II | 4563.76 | 1.22 | -0.96 | 77.4 | 1.53 |
| Ti II | 4571.97 | 1.57 | -0.53 | 86.7 | 1.73 |
| Ti II | 5188.68 | 1.58 | -1.21 | 64.8 | 2.24 |
| Ti II | 5336.77 | 1.58 | -1.70 | 43.7 | 2.32 |
| Cr I | 5206.04 | 0.94 | 0.02 | 74.6 | 2.31 |
| Cr I | 5208.42 | 0.94 | 0.16 | 79.2 | 2.24 |
| Fe I | 4071.74 | 1.61 | -0.02 | 129.9 | 3.93 |
| Fe I | 4132.06 | 1.61 | -0.65 | 102.0 | 3.91 |
| Fe I | 4143.87 | 1.56 | -0.51 | 136.6 | 4.46 |
| Fe I | 4187.04 | 2.45 | -0.55 | 71.8 | 4.27 |
| Fe I | 4202.03 | 1.49 | -0.71 | 107.8 | 3.92 |
| Fe I | 4250.79 | 1.56 | -0.71 | 110.8 | 4.05 |
| Fe I | 4260.47 | 2.40 | 0.08 | 87.0 | 3.82 |

Table 1. (Continued.)

| Species | wavelength(Å) | L.E.P.(eV) | $\log gf$ | W(mÅ) | $\log \epsilon$ |
|---------|---------------|------------|-----------|-------|-----------------|
| Fe I | 4337.05 | 1.56 | -1.70 | 75.6 | 4.36 |
| Fe I | 4383.54 | 1.49 | 0.20 | 168.0 | 4.17 |
| Fe I | 4442.34 | 2.20 | -1.26 | 64.4 | 4.51 |
| Fe I | 4447.72 | 2.22 | -1.34 | 65.5 | 4.64 |
| Fe I | 4459.12 | 2.18 | -1.28 | 58.5 | 4.42 |
| Fe I | 4476.02 | 2.85 | -0.82 | 44.5 | 4.56 |
| Fe I | 4494.56 | 2.20 | -1.14 | 67.0 | 4.42 |
| Fe I | 4528.61 | 2.18 | -0.82 | 85.2 | 4.36 |
| Fe I | 4531.15 | 1.49 | -2.16 | 64.1 | 4.52 |
| Fe I | 4871.32 | 2.87 | -0.36 | 58.7 | 4.29 |
| Fe I | 4872.14 | 2.88 | -0.57 | 46.2 | 4.34 |
| Fe I | 4890.75 | 2.88 | -0.39 | 66.0 | 4.44 |
| Fe I | 4891.49 | 2.85 | -0.11 | 75.2 | 4.27 |
| Fe I | 4903.31 | 2.88 | -0.93 | 28.2 | 4.39 |
| Fe I | 4918.99 | 2.85 | -0.34 | 56.0 | 4.21 |
| Fe I | 4920.50 | 2.83 | 0.07 | 87.8 | 4.25 |
| Fe I | 4939.69 | 0.86 | -3.25 | 69.7 | 4.86 |
| Fe I | 4957.60 | 2.81 | 0.23 | 93.4 | 4.15 |
| Fe I | 4994.13 | 0.92 | -3.08 | 65.6 | 4.70 |
| Fe I | 5006.12 | 2.83 | -0.64 | 51.0 | 4.41 |
| Fe I | 5012.07 | 0.86 | -2.64 | 106.7 | 4.82 |
| Fe I | 5041.76 | 1.49 | -2.20 | 53.2 | 4.35 |
| Fe I | 5049.82 | 2.28 | -1.42 | 41.4* | 4.37 |
| Fe I | 5079.74 | 0.99 | -3.22 | 58.1 | 4.82 |
| Fe I | 5083.34 | 0.96 | -2.96 | 63.3 | 4.59 |
| Fe I | 5123.72 | 1.01 | -3.07 | 37.6 | 4.39 |
| Fe I | 5142.93 | 0.96 | -3.08 | 51.2 | 4.54 |
| Fe I | 5150.84 | 0.99 | -3.07 | 45.9* | 4.49 |
| Fe I | 5151.91 | 1.01 | -3.32 | 41.3* | 4.69 |
| Fe I | 5166.28 | 0.00 | -4.20 | 69.0 | 4.70 |
| Fe I | 5171.60 | 1.49 | -1.79 | 99.9 | 4.61 |
| Fe I | 5194.94 | 1.56 | -2.09 | 53.9 | 4.32 |
| Fe I | 5216.27 | 1.61 | -2.15 | 57.2 | 4.49 |
| Fe I | 5232.94 | 2.94 | -0.06 | 63.7 | 4.12 |
| Fe I | 5250.65 | 2.20 | -2.05 | 28.5* | 4.66 |
| Fe I | 5266.56 | 3.00 | -0.39 | 36.3 | 4.11 |

Table 1. (Continued.)

| Species | wavelength(Å) | L.E.P.(eV) | $\log gf$ | W(mÅ) | $\log \epsilon$ |
|---------|---------------|------------|-----------|-------|-----------------|
| Fe I | 5269.54 | 0.86 | −1.32 | 158.6 | 4.43 |
| Fe I | 5270.36 | 1.61 | −1.51 | 120.9 | 4.84 |
| Fe I | 5324.18 | 3.21 | −0.24 | 43.1 | 4.32 |
| Fe I | 5328.04 | 0.92 | −1.47 | 154.4 | 4.55 |
| Fe I | 5328.53 | 1.56 | −1.85 | 78.8* | 4.41 |
| Fe I | 5339.93 | 3.27 | −0.68 | 26.0* | 4.53 |
| Fe I | 5341.02 | 1.61 | −2.06 | 78.0 | 4.67 |
| Fe I | 5371.49 | 0.96 | −1.64 | 127.6 | 4.25 |
| Fe I | 5397.13 | 0.92 | −1.99 | 112.1 | 4.26 |
| Fe I | 5405.77 | 0.99 | −1.84 | 121.8 | 4.38 |
| Fe I | 5434.52 | 1.01 | −2.12 | 117.6 | 4.60 |
| Fe I | 5446.92 | 0.99 | −1.93 | 121.2 | 4.44 |
| Fe I | 5455.61 | 1.01 | −2.09 | 125.2 | 4.70 |
| Fe I | 5497.52 | 1.01 | −2.85 | 70.8 | 4.60 |
| Fe I | 5501.46 | 0.96 | −2.95 | 58.2* | 4.47 |
| Fe I | 5506.78 | 0.99 | −2.80 | 82.3* | 4.68 |
| Fe I | 5569.62 | 3.42 | −0.54 | 29.5* | 4.63 |
| Fe I | 5615.64 | 3.33 | −0.14 | 55.0* | 4.52 |
| Fe I | 6136.62 | 2.45 | −1.40 | 37.9* | 4.41 |
| Fe I | 6137.69 | 2.59 | −1.40 | 20.3* | 4.24 |
| Fe I | 6191.56 | 2.43 | −1.60 | 35.1* | 4.54 |
| Fe I | 6430.85 | 2.18 | −2.01 | 31.0* | 4.55 |
| Fe II | 4508.29 | 2.86 | −2.31 | 39.5 | 4.52 |
| Fe II | 4515.34 | 2.84 | −2.48 | 39.5 | 4.67 |
| Fe II | 4583.84 | 2.81 | −1.74 | 59.4 | 4.19 |
| Fe II | 4923.93 | 2.89 | −1.21 | 79.8 | 4.01 |
| Fe II | 5018.43 | 2.89 | −1.23 | 101.1 | 4.35 |
| Fe II | 5197.58 | 3.23 | −2.35 | 17.2 | 4.49 |
| Fe II | 5234.63 | 3.22 | −2.15 | 14.5 | 4.19 |
| Fe II | 5275.99 | 3.20 | −2.13 | 30.8 | 4.54 |
| Fe II | 5316.62 | 3.15 | −2.02 | 33.4 | 4.42 |
| Ni I | 5476.90 | 1.83 | −0.89 | 53.7 | 3.10 |
| Zn I | 4722.15 | 4.03 | −0.39 | 14.6 | 2.10 |
| Zn I | 4810.53 | 4.08 | −0.17 | 23.5 | 2.18 |
| Sr II | 4077.72 | 0.00 | 0.17 | 105.3 | −1.56 |
| Y II | 4883.69 | 1.08 | 0.07 | <37.4 | < −0.57 |

Table 1. (Continued.)

| Species | wavelength(\AA) | L.E.P.(eV) | $\log gf$ | W(m \AA) | $\log \epsilon$ |
|---------|----------------------------|------------|-----------|--------------------|-----------------|
| Zr II | 4317.32 | 0.71 | -1.38 | <46.5 | <1.10 |
| Ba II | 4554.03 | 0.00 | 0.17 | 181.6 | -0.15 |
| Ba II | 4934.08 | 0.00 | -0.15 | 173.6 | -0.19 |
| Ba II | 5853.69 | 0.60 | -0.91 | 69.8* | -0.41 |
| Ba II | 6141.73 | 0.70 | -0.08 | 119.8* | -0.44 |
| La II | 4086.71 | 0.00 | -0.07 | <57.0 | < -1.09 |
| Ce II | 4562.37 | 0.48 | 0.33 | <40.1 | < -0.49 |
| Nd II | 4446.39 | 0.20 | -0.35 | <42.2 | < -0.38 |
| Eu II | 4129.72 | 0.00 | 0.22 | <54.4 | < -1.84 |
| Dy II | 4103.31 | 0.10 | -0.37 | <54.1 | < -0.51 |

* Taken from Aoki et al. (2009).

Table 2. Chemical Abundances of S 15–19

| Species | $\log \epsilon$ | [X/Fe] | N | σ |
|---------|-----------------|--------|----|----------|
| C(CH) | 6.38 | 1.00 | – | 0.3 |
| N(CN) | 6.28 | 1.50 | – | 0.5 |
| Na I | 3.25 | 0.13 | 2 | 0.19 |
| Mg I | 5.05 | 0.57 | 5 | 0.09 |
| Ca I | 3.71 | 0.45 | 6 | 0.15 |
| Sc II | 0.59 | 0.59 | 2 | 0.19 |
| Ti I | 1.96 | 0.11 | 2 | 0.19 |
| Ti II | 1.93 | 0.08 | 9 | 0.27 |
| Cr I | 2.27 | −0.32 | 2 | 0.19 |
| Fe I | 4.43 | −3.02 | 65 | 0.23 |
| Fe II | 4.37 | −3.08 | 9 | 0.21 |
| Ni I | 3.10 | −0.08 | 1 | 0.19 |
| Zn I | 2.14 | 0.59 | 2 | 0.19 |
| Sr II | −1.56 | −1.43 | 1 | 0.19 |
| Y II | < −0.57 | <0.27 | 1 | – |
| Zr II | <1.10 | <1.57 | 1 | – |
| Ba II | −0.43 | 0.44 | 2 | 0.19 |
| La II | < −1.09 | <0.86 | 1 | – |
| Ce II | < −0.49 | <0.98 | 1 | – |
| Nd II | < −0.38 | <1.25 | 1 | – |
| Eu II | < −1.63* | <0.90 | 1 | – |
| Dy II | < −0.51 | <1.44 | 1 | – |

Notes: N indicates the number of lines measured for the determination of abundance, and σ indicates the random error (see text). The upper limit of Eu is determined by spectrum synthesis. [Fe/H] values are given in the column of [X/Fe] for FeI and FeII.

Table 3. Abundances changes from changing stellar parameters

| Species | ΔT_{eff} (+150K) | $\Delta \log g$ (+0.3dex) | $\Delta[\text{Fe}/\text{H}]$ (+0.3 dex) | Δv_{micro} (+0.3km) | Total (dex) |
|---------|------------------------------------|------------------------------|--|---------------------------------------|----------------|
| C(CH) | 0.35 | −0.13 | +0.03 | −0.01 | 0.37 |
| N(CN) | 0.19 | −0.10 | −0.07 | 0.00 | 0.21 |
| Na I | 0.15 | −0.04 | −0.03 | −0.14 | 0.21 |
| Mg I | 0.15 | −0.07 | −0.01 | −0.07 | 0.18 |
| Ca I | 0.10 | −0.02 | −0.01 | −0.02 | 0.11 |
| Sc II | 0.10 | 0.06 | −0.02 | −0.15 | 0.19 |
| Ti I | 0.17 | −0.02 | 0.00 | −0.02 | 0.17 |
| Ti II | 0.06 | 0.08 | 0.00 | −0.07 | 0.13 |
| Cr I | 0.17 | −0.03 | −0.01 | −0.05 | 0.18 |
| Fe I | 0.17 | −0.03 | −0.01 | −0.07 | 0.19 |
| Fe II | 0.00 | 0.10 | 0.00 | −0.03 | 0.10 |
| Ni I | 0.17 | −0.02 | −0.01 | −0.03 | 0.17 |
| Zn I | 0.06 | 0.05 | 0.00 | −0.01 | 0.08 |
| Sr II | 0.11 | 0.07 | −0.02 | −0.16 | 0.20 |
| Y II | 0.08 | 0.09 | 0.01 | −0.02 | 0.12 |
| Zr II | 0.09 | 0.08 | 0.01 | −0.03 | 0.13 |
| Ba II | 0.12 | 0.08 | −0.01 | −0.09 | 0.17 |
| La II | 0.12 | 0.08 | 0.00 | −0.04 | 0.15 |
| Ce II | 0.12 | 0.09 | 0.01 | −0.02 | 0.15 |
| Nd II | 0.12 | 0.08 | 0.01 | −0.02 | 0.15 |
| Eu II | 0.12 | 0.09 | 0.01 | 0.00 | 0.15 |
| Dy II | 0.12 | 0.08 | 0.01 | −0.04 | 0.15 |

Notes: The total error is obtained by adding four uncertainties in quadrature.